Phys. Biol. **5** (2008) 046006 (7pp) doi:10.1088/1478-3975/5/4/046006

A mathematical analysis of second messenger compartmentalization

Wen Chen, Herbert Levine and Wouter-Jan Rappel

Center for Theoretical Biological Physics and Department of Physics, University of California at San Diego, La Jolla, CA 92093-0374, USA

E-mail: hlevine@ucsd.edu

Received 11 July 2008
Accepted for publication 28 October 2008
Published 10 December 2008
Online at stacks.iop.org/PhysBio/5/046006

Abstract

Intracellular compartmentalization of second messengers can lead to microdomains of elevated concentration that are thought to be involved in ensuring signaling specificity. Most experimental evidence for this compartmentalization involves the second messenger adenosine monophosphate (cAMP), which is degraded by phosphodiesterases (PDEs). One possible way of creating these compartments, supported by recent experiments, is to spatially separate the source of cAMP from regions of elevated PDE concentration. To quantify this possibility, we study here a simplified geometry in two dimensions (2D) and in three dimensions (3D), containing a cAMP point source and regions with different degradation constants. Using the symmetry of our geometry, we are able to derive steady state solutions for the cAMP concentration as a function of the system parameters. Furthermore, we show, using analytics as well as direct numerical simulations, that for physiologically relevant time scales the steady state solution has been reached. Our results indicate that elevating the degradation constant throughout the cell, except for a small microdomain surrounding the source, requires an unphysiologically high cellular PDE concentration. On the other hand, a tight spatial relationship of localized PDEs with the cAMP source can result in functional microdomains while maintaining a physiologically plausible cellular PDE concentration.

S This article has associated online supplementary data files

1. Introduction

It has long been known that a large number of signaling pathways can share a common second messenger, generated through a variety of different external stimuli. Obviously, this leads to the potential of cross-talk between these pathways in which an external stimulation excites multiple pathways in an indiscriminate manner. One possibility to avoid this cross-talk and thus ensure pathway specificity is to create spatial regions in which the concentration of the second messenger is markedly different. By spatially localizing the targets of the second messenger in these microdomains it would be possible to excite different pathways for different external stimuli.

Most of the evidence for this compartmentalization comes from work studying cyclic adenosine monophosphate (cAMP) pathways. cAMP is a ubiquitous second messenger, involved in a multitude of processes including differentiation, development, and excitation/contraction coupling in muscle cells. cAMP primarily activates the cAMP-dependent protein kinase (PKA) and is generated by membrane bound adenylyl cyclases (ACs) which, in turn, are activated by transmembrane receptors [1]. Experimental evidence has demonstrated that different stimuli can result in the activation of different downstream pathways [2]. In other words, cAMP-dependent pathways can be activated in a selective and specific fashion. This is surprising since cAMP is a small molecule with a large diffusion coefficient and thus any local elevation in cAMP concentration should rapidly lead to a homogeneous increase in cytosolic cell-wide cAMP levels.

The existence of cAMP microdomains was demonstrated in recent high resolution fluorescence resonance energy transfer (FRET) experiments with submicrometer resolution. These experiments showed that cardiac myocytes, following β-adrenergic stimulation, displayed multiple discrete microdomains of high cAMP concentration [3]. This compartmentalization is thought to play an important role

in functional differences between β_1-adrenergic and β_2-adrenergic signaling [2, 4–6] and might be impaired during heart failure. Similar spatial cAMP gradients have also been found in human embryonic kidney cells [7] and hippocampal neurons [8].

Two scenarios to limit the spatial extent of the second messenger, and thus ensure specificity, have been postulated. In the first, the cell geometry creates anatomical barriers that naturally limit the diffusion of cAMP. In the second scenario, the degradation of cAMP by phosphodiesterases (PDEs) acts to create a 'functional' compartment [9]. These PDEs exist in many isoenzyme variants and have been shown to act either close to the membrane, in the cytosol or both [10]. Recent experiments have shown that the microdomains of cAMP can be abolished by treating the cells with a PDE inhibitor [11], strongly suggesting that the second scenario plays a dominant role in the creation of cAMP microdomains. In fact, additional experiments have demonstrated that the PDEs themselves are not uniformly distributed throughout the cell [12, 13]. Instead, they appear to be anchored to subcellular structures, possibly through A-kinase anchoring protein (AKAP) [14].

Several modeling studies have addressed the β-adrenergic pathway in myocytes [15, 16]. What has been lacking to date, however, is a quantitative and analytical investigation of the effect of PDEs on the spatial distribution of cAMP. In this study we will examine a simplified spherically symmetric model in which molecules from a point source, located on an impermeable membrane, diffuse into a space that contains a region of elevated PDE concentration. Note that our model does not address localization effects that might arise from more complicated geometries. This was shown to occur in a recent numerical study in neurons where the different surface-to-volume ratios for the cell body and for the dendrites can lead to significant concentration gradients [17]. In addition, we do not include possible feedback from cAMP on the PDEs, as considered in [17].

In this study, we derive expressions for the steady state concentration in both 2D and 3D and obtain a simple expression that links the critical experimental parameters (the size of the microdomain, the diffusion constant of the second messenger, the production rate and the degradation constant) to a threshold value for PKA activation of the cAMP concentration. We find that a significant lowering of the concentration requires a large value of the degradation constant. If the PDEs are only excluded from the microdomain adjacent to the cAMP source, such a large degradation constant would necessitate cellular PDE concentrations that are unphysiological. On the other hand, our results show that a tight localization of PDEs can also create functional cAMP microdomains and that by limiting the spatial extent of PDEs the cellular PDE concentration can remain in the physiological range.

2. Compartment model

The detailed cellular geometry of the cAMP machinery, including the location of PDEs is complex and not precisely known. Therefore, we have chosen a highly simplified

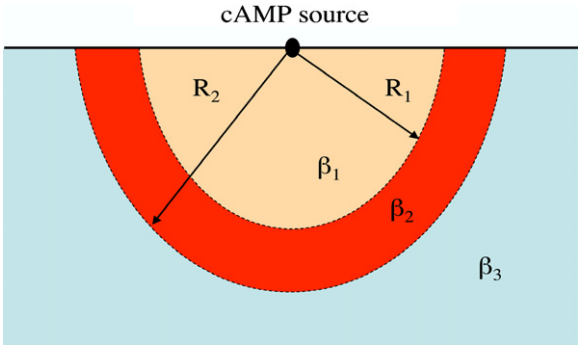

Figure 1. The geometry considered in this paper. A point source emits cAMP molecules into the unbounded half space below the reflecting membrane. The cAMP molecules diffuse freely but the degradation rate β is non-uniform: it is low in the first compartment, of size R_1, and second compartment ($r \geqslant R_2$) but is high in the region $R_1 < r < R_2$.

geometry, depicted in figure 1, that is amenable to an analytical treatment. In this geometry, we consider the cell to occupy the half space below a reflecting boundary. A source is located at the origin, emitting molecules that can diffuse into the cell. As we are interested in the general localization properties of the ensuing diffusion, we do not specify the detailed nature of this source. Furthermore, since we assume that the spatial scale of the source is much smaller that the cell body, we will consider a point source that emits molecules into an infinite domain. The effect of different zones of degradation in the cell is modeled by defining three regions with different degradation constants: a region of radius R_1 with degradation rate β_1, a region $R_1 < r < R_2$ with degradation rate β_2 and a region which extends beyond R_2 and which has a degradation constant β_3. Of course, since we are investigating scenarios where the degradation constant can form microdomains, we will be most interested in the case where β_2 is much larger than β_1.

The concentrations in the microdomain, C_1, in the high degradation zone, C_2, and in the remainder of the cytosol, C_3, obey the diffusion equation

$$\begin{aligned} \frac{\partial C_1}{\partial t} &= D\nabla^2 C_1 - \beta_1 C_1, & 0 \leqslant r \leqslant R_1 \\ \frac{\partial C_2}{\partial t} &= D\nabla^2 C_2 - \beta_2 C_2, & R_1 < r < R_2 \\ \frac{\partial C_3}{\partial t} &= D\nabla^2 C_3 - \beta_3 C_3, & r \geqslant R_2. \end{aligned} \tag{1}$$

At the boundary separating the three regions, both the concentration and its derivative must be continuous

$$C_1(R_1, t) = C_2(R_1, t) \qquad C_2(R_2, t) = C_3(R_2, t) \tag{2}$$

$$\begin{aligned} \frac{\partial C_1(R_1, t)}{\partial r} &= \frac{\partial C_2(R_1, t)}{\partial r} \\ \frac{\partial C_2(R_2, t)}{\partial r} &= \frac{\partial C_3(R_2, t)}{\partial r} \end{aligned} \tag{3}$$

while far from the source we have

$$C_3(\infty, t) = 0. \tag{4}$$

Finally, we assume that the initial concentration is zero throughout the domain:

$$C_1(r,0) = C_2(r,0) = C_3(r,0) = 0. \tag{5}$$

3. Analytical steady state solution

3.1. Two dimensions

The steady state solution for the concentration field in two dimensions can be found using the angular symmetry and writing the diffusion equation in polar coordinates. In these coordinates, the proper boundary condition for a constant source of F molecules s^{-1} reads

$$\lim_{r\to 0} r\frac{\partial C_1}{\partial r} = -\frac{F}{\pi D}. \tag{6}$$

This, along with the boundary conditions at $r = R_1$ and $r = R_2$, can be used to find a general solution in terms of the flux F, the diffusion constant D, the degradation constants β_1, β_2 and β_3 and the radii of the compartments

$$\begin{aligned} C_1(r) &= \frac{F}{\pi D}\left(A_1\frac{K_0(\alpha_1 r)}{K_0(\alpha_1 R_1)} + A_2\frac{I_0(\alpha_1 r)}{I_0(\alpha_1 R_1)}\right)\\ C_2(r) &= \frac{F}{\pi D}\left(B_1\frac{K_0(\alpha_2 r)}{K_0(\alpha_2 R_2)} + B_2\frac{I_0(\alpha_2 r)}{I_0(\alpha_2 R_2)}\right)\\ C_3(r) &= \frac{F}{\pi D}(B_1+B_2)\frac{K_0(\alpha_3 r)}{K_0(\alpha_3 R_2)}, \end{aligned} \tag{7}$$

where $\alpha_i = \sqrt{\frac{\beta_i}{D}}$ for $i = 1, 2, 3$. Here, and in the remainder of the paper, I_n and K_n represent the modified Bessel function of the first kind and second kind of order n (see, e.g., [18]). The coefficients are given by

$$\begin{aligned} A_1 &= K_0(\alpha_1 R_1)\\ B_1 &= \frac{dA_1}{b+ac}\\ B_2 &= aB_1\\ A_2 &= \frac{K_0(\alpha_2 R_1)}{K_0(\alpha_2 R_2)}B_1 + \frac{I_0(\alpha_2 R_1)}{I_0(\alpha_2 R_2)}B_2 - A_1 \end{aligned}$$

with

$$\begin{aligned} a &= \frac{\frac{\alpha_2 K_1(\alpha_2 R_2)}{K_0(\alpha_2 R_2)} - \frac{\alpha_3 K_1(\alpha_3 R_2)}{K_0(\alpha_3 R_2)}}{\frac{\alpha_2 I_1(\alpha_2 R_2)}{I_0(\alpha_2 R_2)} + \frac{\alpha_3 K_1(\alpha_3 R_2)}{K_0(\alpha_3 R_2)}}\\ b &= \alpha_1\frac{I_1(\alpha_1 R_1)K_0(\alpha_2 R_1)}{I_0(\alpha_1 R_1)K_0(\alpha_2 R_2)} + \alpha_2\frac{K_1(\alpha_2 R_1)}{K_0(\alpha_2 R_1)}\\ c &= \alpha_1\frac{I_1(\alpha_1 R_1)I_0(\alpha_2 R_1)}{I_0(\alpha_1 R_1)I_0(\alpha_2 R_2)} - \alpha_2\frac{I_1(\alpha_2 R_1)}{I_0(\alpha_2 R_2)}\\ d &= \alpha_1\left(\frac{K_1(\alpha_1 R_1)}{K_0(\alpha_1 R_1)} + \frac{I_1(\alpha_1 R_1)}{I_0(\alpha_1 R_1)}\right). \end{aligned}$$

Note that for the special case of uniform degradation $\alpha_1 = \alpha_2 \equiv \alpha$ the solution simplifies to

$$C_{\text{uni}}(r) = \frac{F}{\pi D}K_0(\alpha r). \tag{8}$$

3.2. Three dimensions

In three dimensions the diffusion equations can be written in spherical coordinates while the proper flux condition reads

$$\lim_{r\to 0} r^2\frac{\partial c_1}{\partial r} = -\frac{F}{2\pi D}. \tag{9}$$

Now, the solution is written in terms of modified spherical Bessel functions k_n and i_n [18]. To distinguish our 3D steady state results from the 2D results we will denote the 3D solutions in lower case

$$\begin{aligned} c_1(r) &= \frac{F}{2\pi D}\left(A_1'\frac{k_0(\alpha_1 r)}{k_0(\alpha_1 R_1)} + A_2'\frac{i_0(\alpha_1 r)}{i_0(\alpha_1 R_1)}\right)\\ c_2(r) &= \frac{F}{2\pi D}\left(B_1'\frac{k_0(\alpha_2 r)}{k_0(\alpha_2 R_2)} + B_2'\frac{i_0(\alpha_2 r)}{i_0(\alpha_2 R_2)}\right)\\ c_3(r) &= \frac{F}{2\pi D}(B_1'+B_2')\frac{k_0(\alpha_3 r)}{k_0(\alpha_3 R_2)}. \end{aligned}$$

The expressions for the coefficients are identical to those in 2D with K_n and I_n replaced by k_n and i_n, respectively and with

$$A_1' = \alpha_1 k_0(\alpha_1 R_1).$$

For completeness, we also give the solution for uniform degradation

$$c_{\text{uni}}(r) = \frac{F\alpha}{2\pi D}k_0(\alpha r) \tag{10}$$

and for free diffusion ($\alpha_1 = \alpha_2 = \alpha_3 = 0$)

$$c_{\text{free}}(r) = \frac{F}{2\pi D}\frac{1}{r}. \tag{11}$$

4. Results and discussion

4.1. $R_2 \to \infty$

We first address the case of an infinite compartment with high degradation, i.e. $R_2 \to \infty$. In this case, the steady state solutions can be simplified considerably, leading to

$$\begin{aligned} C_1(r) &= \frac{F}{\pi D}\left(A_1\frac{K_0(\alpha_1 r)}{K_0(\alpha_1 R)} + A_2\frac{I_0(\alpha_1 r)}{I_0(\alpha_1 R)}\right)\\ C_2(r) &= \frac{F}{\pi D}(A_1+A_2)\frac{K_0(\alpha_2 r)}{K_0(\alpha_2 R)} \end{aligned} \tag{12}$$

with

$$A_1 = K_0(\alpha_1 R) \tag{13}$$

$$A_2 = \frac{\alpha_1 K_0(\alpha_2 R)K_1(\alpha_1 R)I_0(\alpha_1 R) - \alpha_2 K_0(\alpha_1 R)K_1(\alpha_2 R)I_0(\alpha_1 R)}{\alpha_1 I_1(\alpha_1 R)K_0(\alpha_2 R) + \alpha_2 K_1(\alpha_2 R)I_0(\alpha_1 R)}, \tag{14}$$

where we have defined $R \equiv R_1$. The 3D solutions can be found from these expression by replacing K_n and I_n with k_n and i_n, the prefactor with $F/(2\pi DR)$ and A_1 with A_1'. In figure 2(*A*) we show the concentration, normalized by the prefactor of equation (12), as a function of the radial distance from the source for several values of the degradation constant β_2. The first compartment has radius $R = 0.1$ μm,

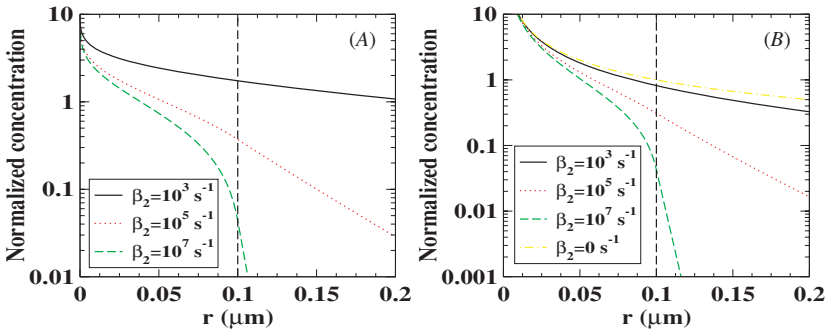

Figure 2. Results for $R_2 \to \infty$. The concentration as a function of the distance from the source in 2D (*A*); normalized by $F/(\pi D)$ and in 3D (*B*); normalized by $F/(2\pi DR)$ for different values of the degradation constant. The compartment size is indicated by the dashed line and was chosen to be $R = 0.1$ μm. For $r \leqslant R$ the degradation constant was set to zero while for $r > R$ it was chosen to be β_2.

indicated by the dashed line, and was chosen to have a negligible degradation constant. As expected, the effect of the degradation in the second compartment becomes more pronounced for larger values of the degradation constant.

In figure 2(*B*) we show a similar set of curves, but now for the 3D case. Again, the concentration profile is normalized by the prefactor $(F/(2\pi DR))$ and is markedly altered for large values of the degradation constant. As a comparison, we have also plotted the concentration for the free diffusion case (i.e., $\beta_i = 0$). Note that such a comparison cannot be made in 2D since there the free diffusion profile diverges ($C_{\text{free}} \sim \ln(r)$).

Obviously, the presence of a nonzero degradation constant reduces the concentration, especially for large values of β_2. To quantify the effect of the degradation in 3D, we can calculate the ratio of the concentration at $r = R, c(R) \equiv c_1(R) = c_2(R)$, for nonzero β_2 and for $\beta_2 = 0$

$$\frac{c(R)}{c_{\text{free}}(R)} = \frac{1}{\alpha_2 R}\frac{k_0(\alpha_2 R)}{k_1(\alpha_2 R)}. \tag{15}$$

For large values of $\alpha_2 R$ this becomes

$$\frac{c(R)}{c_{\text{free}}(R)} \sim \sqrt{\frac{D}{\beta_2}}\frac{1}{R}. \tag{16}$$

This result shows that, as expected, the difference between free diffusion and diffusion in the presence of a high degradation region increases as the degradation constant is increased.

To further determine the effect of high degradation rates in the second compartment we compare the value of the concentration at $r = R$ to a threshold value ϵ. After all, the desired effect of the second region is to create a compartment in which the concentration of cAMP is high enough to activate downstream pathways while decreasing the concentration in the second compartment such that it is lower than this activation threshold. In the limit $\alpha_1 \to 0$, the expression for concentration at $r = R$ in 2D, $C(R) \equiv C_1(R) = C_2(R)$, simplifies to

$$C(R) \sim \frac{F}{\pi D}\frac{K_0(\alpha_2 R)}{\alpha_2 R K_1(\alpha_2 R)} \tag{17}$$

with an equivalent expression in 3D. The resulting threshold condition $C(R) \leqslant \epsilon$ can be further simplified in the limit of large degradation constants ($\alpha_2 R \geqslant 1$). Thus in 2D, we find a minimum value for the degradation constant

$$\beta_2 \gtrsim \frac{F^2}{\pi^2 D\epsilon^2 R^2} \tag{18}$$

and as follows, in 3D we obtain

$$\beta_2 \gtrsim \frac{F^2}{4\pi^2 D\epsilon^2 R^4}. \tag{19}$$

Of course, the expression in 3D is only valid if the concentration for the free diffusion case is above the threshold value. This sets a constraint on the flux, which has to be at least $F_{\min} = 2\pi DR\epsilon$. Again, since its free diffusion case is divergent there is no equivalent constraint in 2D. The above expressions show the expected dependence on the system parameters. For example, for increasing flux one needs to increase the degradation constant. Also, a smaller compartment size requires a larger degradation constant.

To address possible transient effects, we have also obtained an analytical time-dependent two-dimensional solution in the case of a instantaneous flux source in 2D (see supplementary information)

$$\lim_{r\to 0} r\frac{\partial C_1}{\partial r} = -\frac{F}{\pi D}\delta(t). \tag{20}$$

The solution can be found using the method of Laplace transforms and details are given in the supplementary information. The final expressions are given by

$$C_1(r,t) = \frac{F}{\pi D}\left[\frac{1}{2t}\exp\left(-\frac{r^2}{4Dt} - \beta_1 t\right)\right.$$
$$\left. + \sum_{j=1}^{n}\frac{N_1(x_j)}{N'(x_j)} I_0(r k_1(x_j))\exp(x_j t) - \mathcal{L}[F_1(r,s)]\exp(-\beta_2 t)\right]$$

$$C_2(r,t) = \frac{F}{\pi D}\left(\sum_{j=1}^{n}\frac{K_0\left(r\sqrt{\frac{x_j+\beta_2}{D}}\right)}{N'(x_j)}\exp(x_j t)\right.$$
$$\left. - \mathcal{L}[F_2(r,s)]\exp(-\beta_2 t)\right). \tag{21}$$

The first term in C_1 can be recognized as the free diffusion solution. The second term is a sum over all the zeroes x_j of a function N, given in the supplementary information, in the interval $(-\beta_2, \beta_1)$. The final term involves the Laplace

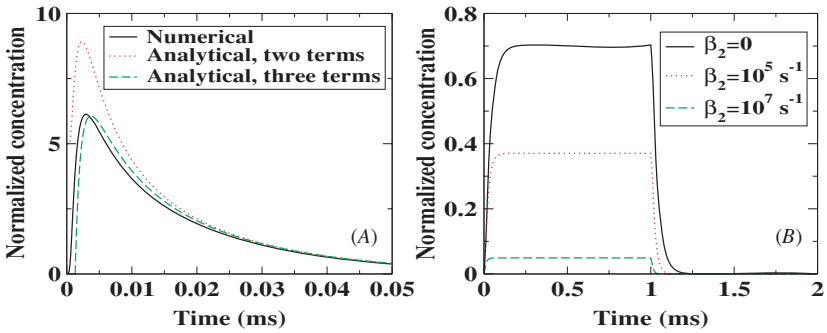

Figure 3. Time-dependent solutions for the concentration field for $R_2 \to \infty$ in 2D. (*A*) The concentration, normalized by $F/(\pi D)$, as a function of time at $r = R/2$ for $R = 0.1$ μm. The flux was turned on at $t = 0$. Shown are the exact numerical solution (black line) and two approximative analytical solutions (see text). (*B*) The numerically obtained concentration at $r = R$, $R = 0.1$ μm, as a function of time for different degradation constants β_2. The source was turned on at $t = 0$ and turned off at $t = 1$ ms.

transform of the function F_1, again given in the supplementary information. Likewise, the expression for C_2 contains a term which is a sum over the zeroes x_j of a function given in the supplementary information, along with a term which is the Laplace transform of F_2, which can be found in the supplementary information.

It is possible to simplify the expression by expanding the Laplace transform for large values of t (see supplementary information). To examine the accuracy of this expansion we have plotted in figure 3(*A*) the normalized concentration at $r = R/2$ as a function of time following a sudden turning on of the flux F at $t = 0$. The red dotted line represents the result using equation (21) without the Laplace transform and the green dashed line shows the results with the first term in the expansion. As a comparison, the black line is the result of the full numerical solution. The figure shows that keeping only the first term in the expansion accurately captures the time dynamics, especially for larger times. In figure 3(*B*) we plot the concentration at $r = R$, assuming a source that releases a constant flux for 1 ms which should be well below the time of activation of AC. Importantly, the concentration in the compartment reaches steady state within 1 ms.

In three dimensions, finding an analytical solution for the dynamic case becomes more difficult. To obtain time-dependent solutions for this geometry we have numerically integrated our equations. Again, we find that the concentration reaches a steady state within 1 ms (data not shown). Taken together, these results demonstrate that to investigate cAMP microdomains in our simple model it is sufficient to examine the steady state response.

4.2. Finite R_2

From the above results, it becomes clear that the degradation rate in the second region needs to be large to ensure a small value of the second messenger concentration at its boundary. This degradation rate can be translated into a cellular PDE concentration when we assume Michaelis–Menten dynamics. If we use simple first-order kinetics, we can approximate the degradation rate as

$$\beta = \frac{k_{\text{cat}}[\text{PDE}]}{K_m + [\text{cAMP}]}, \tag{22}$$

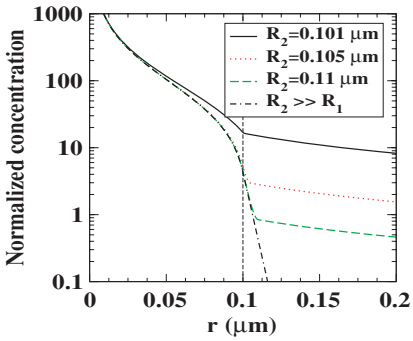

Figure 4. The 3D steady state concentration profile, normalized by $F/(2\pi D R_1)$, for a fixed value of $\beta_2 = 10^7$ s^{-1} and for different values of R_2. The size of the first compartment is $R_1 = 0.1$ μm.

where k_{cat} is the catalytic constant and K_m is the Michaelis–Menten constant. Experimental values for these constants are subject to considerable uncertainty. Nevertheless, if we use reported values ($k_{\text{cat}} = 5$ s^{-1} and $K_m = 1.3$ μm, [19]), based on our model we can rewrite above equation as below (since the concentration beyond the boundary, c_2, is much lower than K_m)

$$\beta_2 = \frac{k_{\text{cat}}[\text{PDE}]}{K_m + c_2} \approx \frac{k_{\text{cat}}[\text{PDE}]}{K_m}. \tag{23}$$

Hence, we find that for the degradation rates presented in figure 2(*B*) require PDE concentrations that are many orders of magnitude larger than K_m and much larger than reported values [19, 20]. Thus, our results suggest that using a uniform high degradation zone is physiologically implausible.

Next, we examined the case of finite R_2 and take, for the sake of simplicity, $\beta_1 = \beta_3 = 0$. Results are shown in figure 4 where we plot the normalized concentration as a function of r in 3D for different values of R_2 and a fixed value of β_2 and R_1. From the figure we can see that the concentration profile within the high degradation compartment approaches the one corresponding to $R_2 \to \infty$ already for small values of $R_2 - R_1$. This can be understood by realizing that when

the size of the high degradation zone is larger than the decay length, i.e. when

$$R_2 - R_1 > \sqrt{\frac{D}{\beta_2}} \tag{24}$$

the size of the region becomes irrelevant. For the parameter values used in figure 4 and for $D = 100\ \mu\text{m}^2\ \text{s}^{-1}$ we find that $\sqrt{\frac{D}{\beta_2}} \sim 0.003\ \mu\text{m}$.

To quantify the effect of the high degradation rate in the second compartment, we can again compare the steady state solution to a threshold value ϵ. In particular, we can determine for which parameter values $c_2(R_2)$ crosses this threshold. In the limit of large $\alpha_2 R_2$ we can again find a simple relationship between this threshold and the relevant system parameters. Apart from a numerical factor of order 1, and assuming that $(R_2 - R_1)/R_1 \ll 1$, these expressions are identical to those shown in equations (18) and (19). It then becomes obvious that localizing the PDEs can, at the same time, produce a region with a large degradation constant while maintaining an overall PDE concentration that is physiologically plausible. In fact, we can estimate the ratio between the PDE concentration in high degradation area and the cellular PDE concentration. This ratio is simply the ratio of the total volume of spherical half shells and the cell volume

$$\frac{[\text{PDE}](\text{finite } R_2)}{[\text{PDE}](R_2 \to \infty)} \sim N_{\text{tot}} \frac{2\pi R_1^2 (R_2 - R_1)}{V_{\text{cell}}}, \tag{25}$$

where N_{tot} is the total number of separate sites emitting cAMP (i.e. the number of spherical half shells). Taking a cell volume of $V_{\text{cell}} = 1.6 \times 10^4\ \mu\text{m}^3$ [21] and using the parameter values of figure 4 with $R_2 - R_1 = 0.01\ \mu\text{m}$ we get that this ratio is approximately $5 \times 10^{-8} N_{\text{tot}}$. Using the reported value of $\sim 10^5$ β-adrenergic receptors per cell [22] for N_{tot} we find that the cellular concentration of PDE can be several orders of magnitude smaller than the concentration within the high degradation compartment.

An accurate estimate of the required degradation constant is difficult without a precise knowledge of the involved parameters. Nevertheless, we can estimate its order of magnitude using a threshold value of $\epsilon = 0.1\ \mu\text{m}$ [23]. Recalling the experiments that show that PDE inhibitors abolish microdomains [11], this threshold should be significantly lower that the value reached via pure diffusion. Hence, the flux should be larger than the aforementioned minimum value $F_{\text{min}} = 2\pi D R \epsilon$. For this value of the threshold, combined with a microdomain size of $R = 0.1\ \mu\text{m}$ and a diffusion constant of $D = 100\ \mu\text{m}^2\ \text{s}^{-1}$ we find a minimum 3D flux rate of at least $F_{\text{min}} \sim 4000$ molecules s^{-1} Comparing this to the turnover rate of AC, which is estimated for the soluble form to be around 10 s^{-1} [24], we find, as in a previous modeling study [25], that the source needs to consist of multiple ACs. Of course, a significant reduction of the diffusion constant, as argued in a recent study [26], might alter this conclusion. Note also that if this source contains multiple receptors the ratio computed above (equation (25)) will become even larger.

Assuming that the flux at our source is $F = 10\,000$ molecules s^{-1}, we find that for $R_2 \to \infty$ the minimum degradation rate is $\beta_2 \sim 10^4\ \text{s}^{-1}$. With the previously quoted catalytic and Michaelis–Menten constants, this would require a local PDE concentration of roughly $2 \times 10^3\ \mu\text{m}$. Clearly, the reduction in the required *cellular* PDE concentration by limiting the spatial extent of the PDEs is able to bring this number into the physiological range. Furthermore, this local concentration of PDEs translates to ~750 PDE molecules in a thin spherical shell of thickness 0.01 μm. Assuming a single layer of PDEs, this would result in an inter-PDE spacing of approximately 0.01 μm, equal to the thickness of the shell. Thus, we can conclude that our study demonstrates that the PDEs need to be localized in the neighborhood of the cAMP sources to ensure a tight control of the spatial extent of the cAMP concentration.

Our approach has made a number of simplifications and is amenable to future extensions. For example, we have assumed simple Michaelis–Menten dynamics and have ignored potentially more complicated interactions between the second messenger and the PDE, including possible feedback loops. Such interactions will certainly alter the dynamics of cAMP but should be easy to implement, at least at the numerical level. Also, we have not explicitly modeled PKA activation, AC activation etc [15, 16] but this can be incorporated easily. Finally, we have neglected the detailed structure of the cell by assuming a simple spherical symmetry. Going beyond this idealized geometry requires currently unavailable detailed anatomical knowledge of the location of the PDEs and the cell geometry. Incorporating these details in a numerical approach is, in principal, straightforward. We do not expect, however, that the main conclusion of this study, that PDEs need to be localized to ensure compartmentalization in cAMP signaling, will be changed by these extensions.

Acknowledgments

This research has been supported by the NSF-sponsored Center for Theoretical Biological Physics (grant nos PHY-0216576 and PHY-0225630).

References

[1] Cooper D M 2003 Regulation and organization of adenylyl cyclases and cAMP *Biochem. J.* **375** 517–29
[2] Steinberg S F and Brunton L L 2001 Compartmentation of G protein-coupled signaling pathways in cardiac myocytes *Ann. Rev. Pharmacol. Toxicol.* **41** 751–73
[3] Zaccolo M and Pozzan T 2002 Discrete microdomains with high concentration of cAMP in stimulated rat neonatal cardiac myocytes *Science* **295** 1711–5
[4] Fischmeister R, Castro L R, Abi-Gerges A, Rochais F, Jurevicius J, Leroy J and Vandecasteele G 2006 Compartmentation of cyclic nucleotide signaling in the heart: the role of cyclic nucleotide phospho-diesterases *Circ. Res.* **99** 816–28
[5] Nikolaev V O, Bunemann M, Schmitteckert E, Lohse M J and Engelhardt S 2006 Cyclic AMP imaging in adult cardiac myocytes reveals far-reaching beta1-adrenergic but locally confined beta2-adrenergic receptor-mediated signaling *Circ. Res.* **99** 1084–91
[6] Leroy J, Abi-Gerges A, Nikolaev V O, Richter W, Lechene P, Mazet J L, Conti M, Fischmeister R and Vandecasteele G

2008 Spatiotemporal dynamics of beta-adrenergic cAMP signals and L-type Ca2+ channel regulation in adult rat ventricular myocytes: role of phosphodiesterases *Circ. Res.* **102** 1091–100

[7] Rich T C, Fagan K A, Tse T E, Schaack J, Cooper D M and Karpen J W 2001 A uniform extracellular stimulus triggers distinct cAMP signals in different compartments of a simple cell *Proc. Natl. Acad. Sci. USA* **98** 13049–54

[8] Davare M A, Avdonin V, Hall D D, Peden E M, Burette A, Weinberg R J, Horne M C, Hoshi T and Hell J W 2001 A beta2 adrenergic receptor signaling complex assembled with the Ca2+ channel Cav1.2 *Science* **293** 98–101

[9] Brunton L L, Hayes J S and Mayer S E 1981 Functional compartmentation of cyclic AMP and protein kinase in heart *Adv. Cyclic. Nucleotide Res.* **14** 391–7

[10] Terrin A *et al* 2006 PGE(1) stimulation of HEK293 cells generates multiple contiguous domains with different [cAMP]: role of compartmentalized phosphodiesterases *J. Cell. Biol.* **175** 441–51

[11] Zaccolo M, Benedetto G D, Lissandron V, Mancuso L, Terrin A and Zamparo I 2006 Restricted diffusion of a freely diffusible second messenger: mechanisms underlying compartmentalized cAMP signalling *Biochem. Soc. Trans.* **34** 495–7

[12] Mongillo M *et al* 2004 Fluorescence resonance energy transfer-based analysis of cAMP dynamics in live neonatal rat cardiac myocytes reveals distinct functions of compartmentalized phosphodiesterases *Circ. Res.* **95** 67–75

[13] Mongillo M *et al* 2006 Compartmentalized phosphodiesterase-2 activity blunts beta-adrenergic cardiac inotropy via an NO/cGMP-dependent pathway *Circ. Res.* **98** 226–34

[14] Wong W and Scott J D 2004 AKAP signalling complexes: focal points in space and time *Nat. Rev. Mol. Cell. Biol.* **5** 959–70

[15] Saucerman J J, Brunton L L, Michailova A P and McCulloch A D 2003 Modeling beta-adrenergic control of cardiac myocyte contractility in silico *J. Biol. Chem.* **278** 47997–8003

[16] Xin W, Tran T M, Richter W, Clark R B and Rich T C 2008 Roles of GRK and PDE4 activities in the regulation of beta2 adrenergic signaling *J. Gen. Physiol.* **131** 349–64

[17] Neves S R *et al* 2008 Cell shape and negative links in regulatory motifs together control spatial information flow in signaling networks *Cell* **133** 666–80

[18] Abramowitz M and Stegun I A 1964 *Handbook of Mathematical Functions with Formulas, Graphs, and Mathematical Tables* (New York: Dover)

[19] Reeves M L, Leigh B K and England P J 1987 The identification of a new cyclic nucleotide phosphodiesterase activity in human and guinea-pig cardiac ventricle. Implications for the mechanism of action of selective phosphodiesterase inhibitors *Biochem. J.* **241** 535–41

[20] Bode D C, Kanter J R and Brunton L L 1991 Cellular distribution of phosphodiesterase isoforms in rat cardiac tissue *Circ. Res.* **68** 1070–9

[21] Takeuchi A, Tatsumi S, Sarai N, Terashima K, Matsuoka S and Noma A 2006 Ionic mechanisms of cardiac cell swelling induced by blocking Na^+/K^+ pump as revealed by experiments and simulation *J. Gen. Physiol.* **128** 495–507

[22] Post S R, Hilal-Dandan R, Urasawa K, Brunton L L and Insel P A 1995 Quantification of signalling components and amplification in the beta-adrenergic-receptor-adenylate cyclase pathway in isolated adult rat ventricular myocytes *Biochem. J.* **311** 75–80

[23] Beavo J A, Bechtel P J and Krebs E G 1974 Activation of protein kinase by physiological concentrations of cyclic AMP *Proc. Natl Acad. Sci. USA* **71** 3580–3

[24] Dessauer C W and Gilman A G 1996 Purification and characterization of a soluble form of mammalian adenylyl cyclase *J. Biol. Chem.* **271** 16967–74

[25] Rich T C, Fagan K A, Nakata H, Schaack J, Cooper D M and Karpen J W 2000 Cyclic nucleotide-gated channels colocalize with adenylyl cyclase in regions of restricted cAMP diffusion *J. Gen. Physiol.* **116** 147–61

[26] Saucerman J J, Zhang J, Martin J C, Peng L X, Stenbit A E, Tsien R Y and McCulloch A D 2006 Systems analysis of PKA-mediated phosphorylation gradients in live cardiac myocytes *Proc. Natl Acad Sci. USA* **103** 12923–8